Heliyon 5 (2019) e02352

Contents lists available at ScienceDirect

Heliyon

journal homepage: www.heliyon.com

Heliyon

Magnetic nanoparticle - indium phthalocyanine conjugate embedded in electrospun fiber for photodynamic antimicrobial chemotherapy and photodegradation of methyl red

Azole Sindelo, Tebello Nyokong *

Institute for Nanotechnology Innovation, Department of Chemistry, Rhodes University, Grahamstown, 6140, South Africa

ARTICLE INFO

Keywords:
Nanotechnology
Materials chemistry
Electrospinning
Polyacrylonitrile
Singlet oxygen quantum yield
Photo-degradation
Photodynamic antimicrobial chemotherapy
Photocatalysis
Nanoparticles
Nanoparticle synthesis
Water pollution
Antibiotic resistant bacteria

ABSTRACT

ClIn(III) octacarboxy phthalocyanine (ClInOCPc) when alone or conjugated to magnetic nanoparticles (MNP-ClInOCPc) was employed for both photodynamic antimicrobial chemotherapy of an unknown water sample and *Staphylococcus aureus*, and for photo-degradation of methyl red (MR). The singlet oxygen quantum yields (Φ_Δ) in water using ClInOCPc and MNP-ClInOCPc embedded in polyacrylonitrile (PAN) electrospun fibers were 0.36 and 0.22, respectively. When in solution, MNP-ClInOCPc gave 90.6% photoinactivation of microbes in a water sample from the stream and of ClInOCPc resulted in 84.8 % photoinactivation. When embedded to the polymer, there was 48.0% clearance for ClInOCPc and 63.7% clearance for MNP-ClInOCPc for the microbes in the water sample from the stream. For the photo-degradation of MR, the rate of degradation increased with decrease of the MR concentration with the MNP-ClInOCPc having the fastest rate.

1. Introduction

Metallophthalocyanines (MPcs) are compounds with various applications in different areas of research including catalysis, photodynamic therapy (PDT), chemical sensors, light-emitting diodes, liquid crystals, laser dyes, nonlinear optics, photodynamic antimicrobial chemotherapy (PACT) and photodegradation of pollutants including azo dyes [1, 2, 3]. In this work, we employed a phthalocyanine as a dual-active material capable of photodegrading an azo dye (methyl red) and in participating in PACT.

In PACT a photoexcited photosensitizer produces reactive oxygen species (ROS) such as singlet oxygen, that are cytotoxic to the targeted bacteria [3]. Some pathogens have become drug resistant, including Methicillin-resistant *Staphylococcus aureus* (MRSA) [4]. PACT has the potential to eliminate the problem of drug resistance. In this work, we use a phthalocyanine linked to magnetic nanoparticles (MNPs) for PACT against *Staphylococcus aureus* (a Gram (+) bacteria). ROS generated by MPcs may also be used for the degradation of pollutants such as azo dyes.

Photocatalysis is one of the prominent methods in the degradation of organic dyes such as azo dyes [5]. Azo dyes are the most common group of synthetic colorants that are widely used in industries such as textiles [6]. There is a great environmental concern about the fate of these dyes, where large amounts enter wastewater streams during industrial operations [5].

MPcs have the ability of generate singlet oxygen [7] which makes them ideal as photosensitizers for PACT and photodegradation of pollutants. The MPc employed in this work is ClIn(III) octacarboxy phthalocyanine (ClInOCPc, insert in Fig. 1A). Indium is employed as a heavy central metal, since it encourages intersystem crossing to the triplet state resulting in increased singlet oxygen generation. In this work, ClInOCPc is covalently linked to MNPs. The photophysical behavior of ClInOCPc and its conjugate will be evaluated as well as their PACT and photodegradation (against methyl red) activities. The MNPs are employed to allow for magnetic separation of the photosensitizers following use. ClInOCPc has been linked to MNPs for photophysical studies [8]. This work presents the use of this conjugate for PACT and photodegradation of pollutants for the first time. It is also the first time that a Pc is employed for PACT using water samples from local streams. There are numerous publications that have tested multiple water samples such as tap water, boiled water and streams [9, 10] and have identifies multiple microbes

* Corresponding author.
E-mail address: t.nyokong@ru.ac.za (T. Nyokong).

https://doi.org/10.1016/j.heliyon.2019.e02352
Received 15 April 2019; Received in revised form 10 July 2019; Accepted 19 August 2019

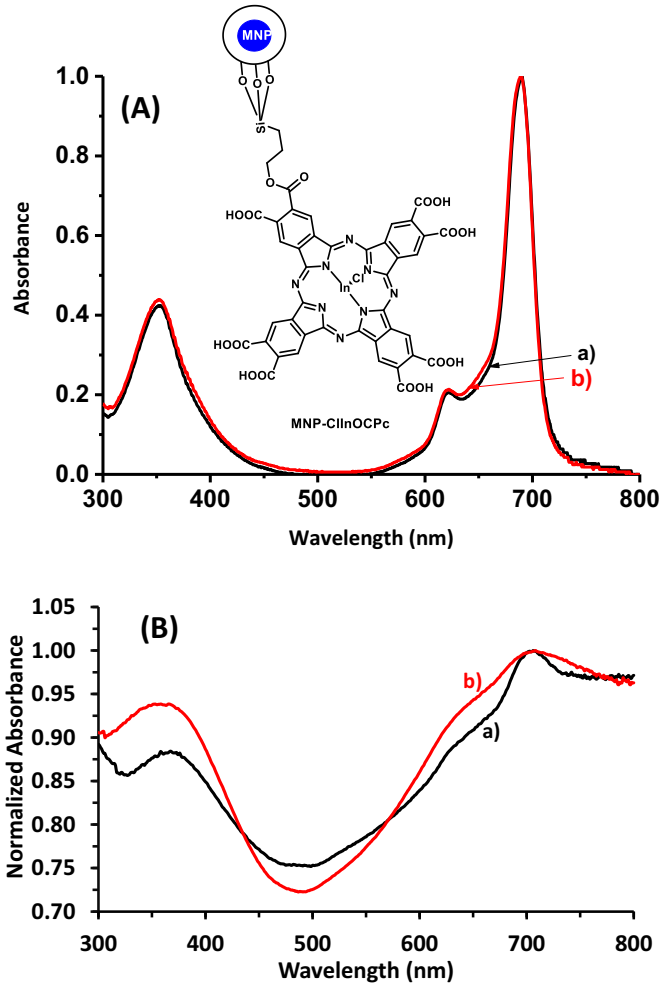

Fig. 1. UV-Vis spectra of (A) ClInOCPc (a) and MNP-ClInOCPc (b) in 0.1 M NaOH. Insert = Representation of the MNP-ClInOCPc, and (B)ClInOCPc/PAN (a) and MNP-ClInOCPc/PAN (b) in the solid state.

such as *Escherichia, Klebsiella, Staphylococcus* and other gram negative and positive species.

Both Pc alone and its conjugate with MNPs are embedded in polyacrylonitrile (PAN) electrospun fibers, represented as ClInOCPc/PAN, MNP-ClInOCPc/PAN, respectively. Thus, recovery of the catalyst is ensured by both the magnetic separation and by the use of electrospun fibers. Electrospinning is commonly used for incorporation of molecules into solid polymer fiber supports [11, 12].

2. Materials and methods

2.1. Materials

The following materials were obtained from Sigma-Aldrich (Johannesburg, South Africa): polyacrylonitrile (PAN, MW = 150 000 g/mol), zinc phthalocyanine (ZnPc), anthracene-9,10-bismethylmalonate (ADMA) and 1,3-diphenylisobenzofuran (DPBF). Dimethylformamide (DMF) was from Associated Chemical Enterprises (Johannesburg, South Africa). Methyl red (MR), nutrient agar and bacteriological BBL Muller Hinton broth were purchased from Merck. *S. aureus* (ATCC 25923) was from Davies Diagnostics (Randburg, South Africa). Phosphate buffer saline (10 mM PBS) pH 7.4 was employed for aqueous solutions. The synthesis of ClInOCPc and its conjugation to MNPs has been reported [8]. This involves coupling the COOH group of ClInOCPc to NH_2 group of MNPs using N-hydroxysuccinimide (NHS), N-(3-dimethylaminopropyl)-N′-ethylcarbodiimide hydrochloride (EDC) chemistry.

Table 1
BET, DLS, photophysical and photochemical parameters for ClInOCPc and its conjugates. Solvent DMF unless otherwise stated.

Sample	DLS size (nm)	BET area (m^2g)[a]	Q band (nm)	Φ_T	τ_T (μs)	Φ_Δ
MNPs	38.0	-	-	-	-	-
ClInOCPc	-	-	689	0.69	115	0.61 0.41[c]
MNP-ClInOCPc	43.8	-	689	0.83	246	0.48 0.29[c]
PAN	-	17.0 (0.11)	-	-		-
ClInOCPc/PAN	-	22.6 (0.11)	702[b]	-		0.22[c]
MNP-ClInOCPc/PAN	-	37.3 (0.18)	702[b]	-		0.36[c]

[a] BET volume in brackets (cm^3/g).
[b] Solid state spectra.
[c] Values in water.

The synthesis of ClAlPcSmix was according to reported methods [13]. This involves refluxing ClAlPc in fuming sulfuric acid. The water samples were collected from Rhodes University Botanical Gardens stream situated at 33°18′58.7″S and 26°31′13.5″E. The samples were collected in March 2017. The electrospun fibers were immersed in the methyl red solutions or water samples for 30 min prior to the photocatalytic experiments being carried out, to eliminate adsorption effect.

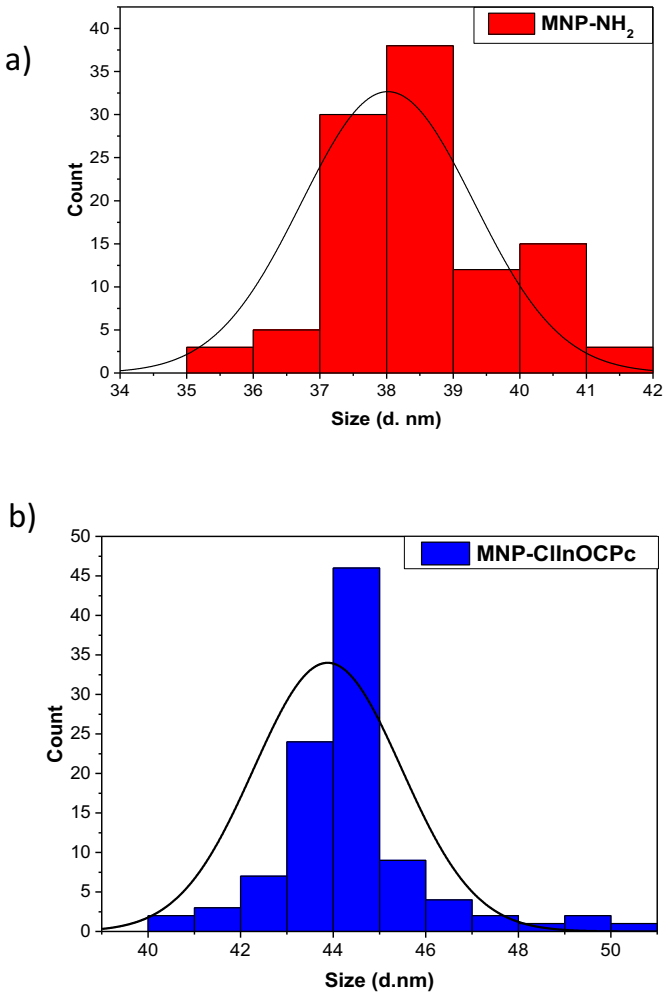

Fig. 2. DLS plots of (a) MNP-NH_2 and (b) MNP-ClInOCPc in DMSO.

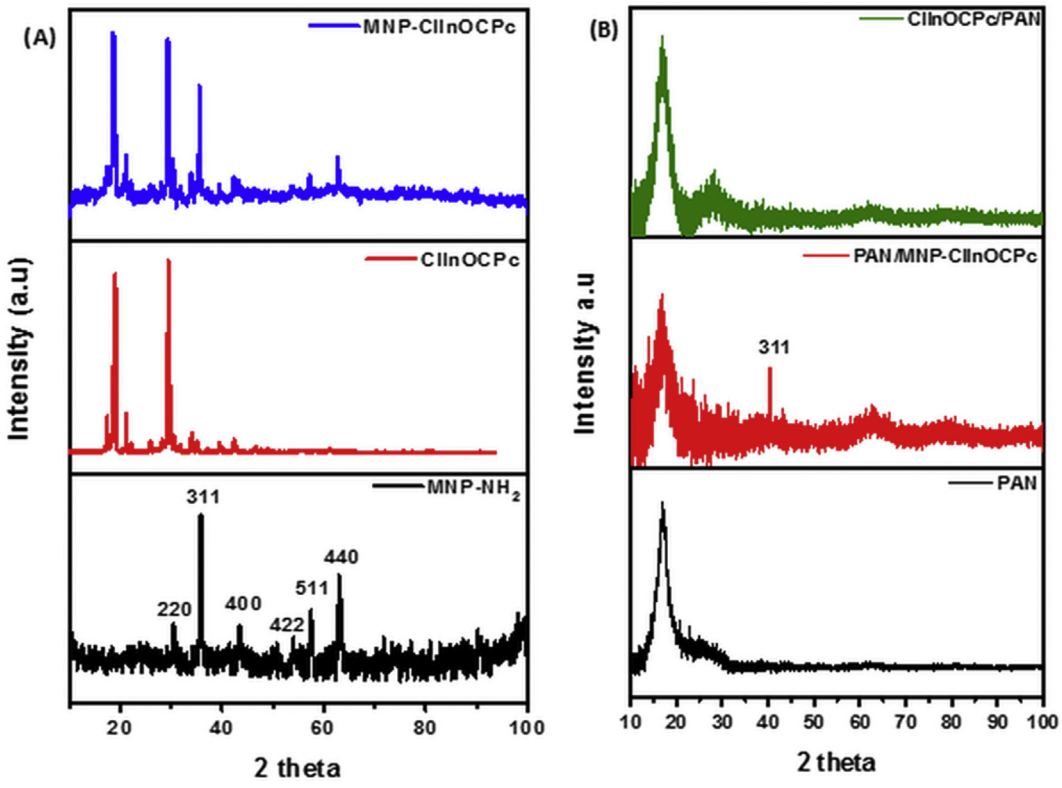

Fig. 3. XRD diffractograms of (A) MNP-ClInOCPc, ClInOCPc and MNP-NH_2 and (B)PAN, MNP-ClInOCPc/PAN and ClInOCPc/PAN.

2.2. Equipment

A Shimadzu UV–Vis 2550 spectrophotometer was employed for UV-Vis spectra in solution and Perkin Elmer Lambda 950 UV-vis spectrophotometer for solid state spectra. JEOL JSM 840 scanning electron microscope (SEM), Zeiss Libra 120 transmission electron microscope (TEM), and INCA PENTA FET energy dispersive X-ray spectroscopy (EDX) were employed. Malvern Zetasizer Nano-ZS90 was used for dynamic light scattering (DLS) in DMSO.

Bruker D8 Discover diffractometer was used for X-ray diffractograms (XRD) data [8]. Laser flash photolysis experiments were performed as explained before [8]. Irradiations for singlet oxygen quantum yield

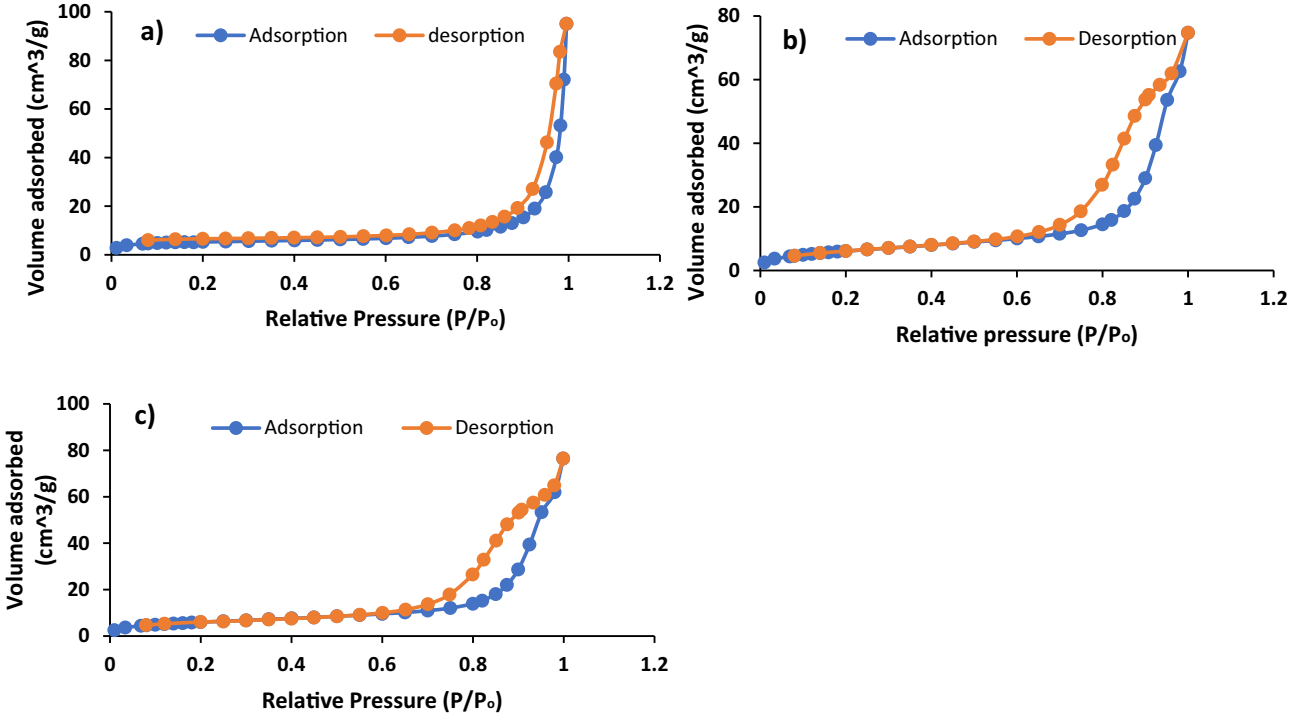

Fig. 4. BET adsorption and desorption graphs of (a) PAN, (b) ClInOCPc/PAN and (c) MNP-ClInOCPc/PAN.

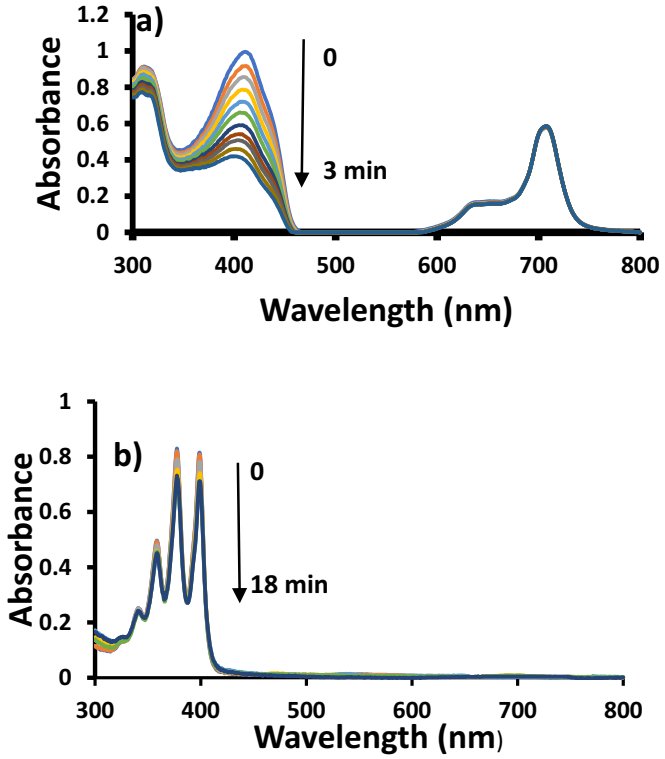

Fig. 5. The UV-vis spectra showing changes during degradation of DPBF (a) in the presence of ClInOCPc in DMF and ADMA (b) in the presence of ClInOCPc/PAN suspended in water.

determinations and PACT as well as the preparation of bacteria were performed as explained before [14]. Photo-degradation of methyl red was performed using Modulight ® Medical Laser system (ML) 7710-680. Micrometrics ASAP 2020 Surface Area and Porosity Analyzer was employed for nitrogen adsorption/desorption isotherms [14].

2.3. Electrospinning procedures

Polyacrylonitrile (PAN) powder was dissolved in DMF and stirred for 24 h at room temperature. The electrospun unfunctionalised PAN fibers were prepared by placing the solution in a 5 mL syringe fitted with a hypodermic needle (inner diameter of 0.1 mm). Electrospinning was then conducted at a flow rate of 0.05 mL/h, voltage = 15 kV, tip to collector distance of 12 cm at room temperature and with relative humidity of 48%.

For the modified PAN fiber, ClInOCPc (2 mg) or MNP-ClInOCPc (3.7 mg) were added to the polymer solution and stirred overnight. The electrospun fibers were then prepared using the same parameters as outlined above for PAN alone to give ClInOCPc/PAN, MNP-ClInOCPc/PAN fiber mats, respectively.

2.4. Photophysical and photochemical parameters

Comparative methods [15] were used for the determination of triplet (Φ_T) and singlet oxygen (Φ_Δ) quantum yields. ZnPc in DMF was used as a standard with: $\Phi_T = 0.58$ [16] and $\Phi_\Delta = 0.56$ [15] (using DPBF chemical quencher, for the latter). In water, ADMA was employed as a quencher for singlet oxygen studies using ClAlPcSmix as a standard ($\Phi_\Delta = 0.42$ [15]). For the determination of Φ_Δ values of ClInOCPc/PAN, and MNP-ClInOCPc/PAN embedded in fiber, the direct chemical method was employed [15].

2.5. Antimicrobial studies

The heat sensitivity of different microorganism differs and the optimal temperature was determined by incubating the sample at different temperatures of 20, 25, 27, 30, 37, 40 °C for 24 and 48 h. pHs of the water sample were adjusted to 2, 4, 6,7.2, 9 and 14, by adding PBS. Optimal temperature and time were 30 °C and 24 h, respectively.

PACT activities of the bacteria were performed using methods previously reported [14].

3. Results and discussion

3.1. Characterization of MNP-ClInOCPc

The synthesis of NH_2 containing MNPs (MNP-NH_2) involves functionalization with silica using tetraethoxysilane (TEOS) followed by addition of 3-aminopropyltriethoxysilane (APTES) [14]. Even though the conjugation of ClInOCPc to MNPs has been reported before [8], a new batch of MNPs was synthesized with different defects and sizes hence the nano-conjugates were characterized. The conjugate is represented in

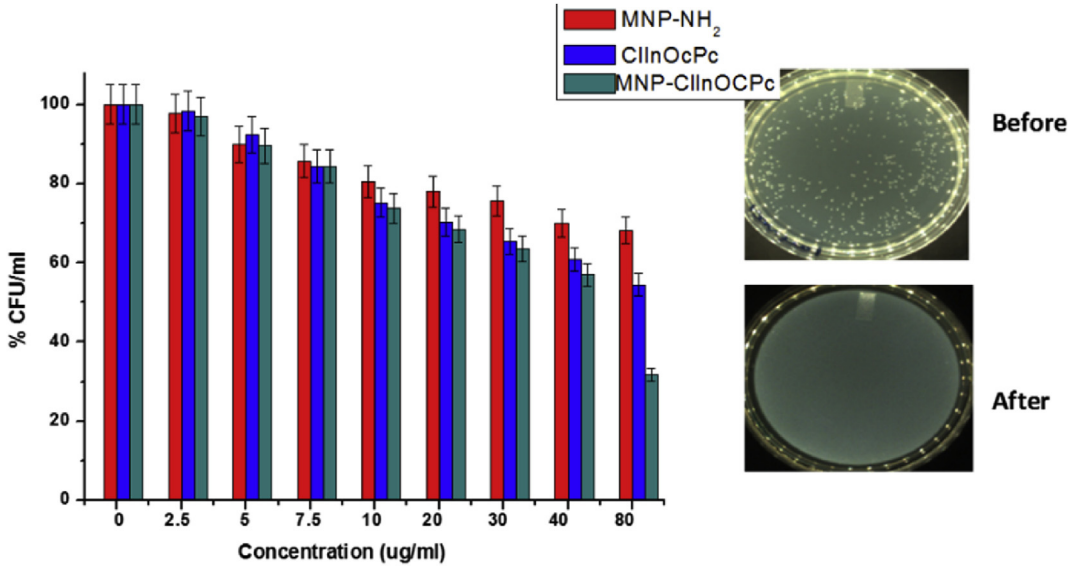

Fig. 6. Dark toxicity studies of the Pcs and conjugate against *S.aureus*. Insert = colony forming photograph of MNP-ClInOCPc before and after PACT.

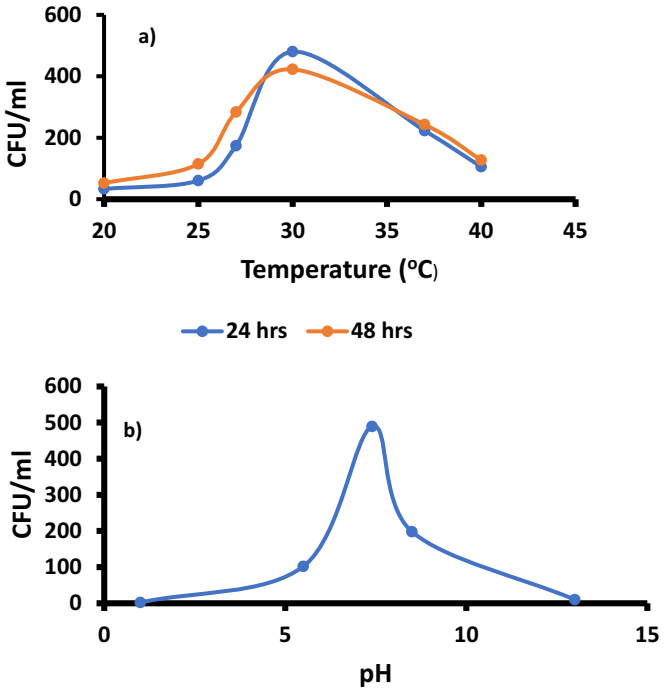

Fig. 7. Optimization studies of a) temperature and b) pH (at 30 °C).

Fig. 1A (as an insert). The spectra of ClInOCPc was recorded in 0.1 M NaOH and there were no shifts in the Q band at 689 nm (Table 1), for ClInOCPc in the presence of MNPs, Fig. 1A.

TEM images of the MNP-NH_2 (*Supporting Information*, Fig. S1, HELION_2019-3366R3-SI.PDF) illustrates that they are spherical in nature with sizes ranging from 30-35 nm and are mono-dispersed. The TEM image of the MNP-ClInOCPc conjugates shows aggregation, which was not observed in the nanoparticle alone. Aggregation upon conjugation could be due to ππ interaction of phthalocyanines [17] from adjacent MNPs. EDX also showed expected elements for MNPs, Pc and conjugates, *Supporting Information*, Fig. S2A, HELION_2019-3366R3-SI.PDF). DLS was employed to determine the hydrodynamic sizes, Fig. 2. The sizes for MNP-NH_2 and MNP-ClInOCPc were 38.0 nm and 43.8 nm, respectively, Table 1. The DLS size for MNP-NH_2 is slightly higher than the range obtained from TEM. Discrepancies in particle sizes determined by TEM and DLS could be attributed to interference of the dispersant into the hydrodynamic diameter [18], resulting in shifts to higher values for the latter. There is an increase in size of the MNP-NH_2 nanoparticles upon conjugation due to aggregation as discussed above.

The XRD diffractograms (XRD, Fig. 3A), show peaks characteristic of magnetite at (220), (311), (400), (422), (511) and (440) as reported before [14]. The XRD pattern for ClInOCPc shows sharp peaks which have been observed before [19, 20]. The conjugate retains the crystallinity of both the ClInOCPc and MNP-NH_2 with slight shifts in the XRD peaks. The XRD data was used to determine the size of the nanoparticles and conjugate employing the Debye-Scherrer equation [21]. The MNP-NH_2 nanoparticle has a size of 33.8 nm, this value is within the range for TEM. After conjugating with the ClInOCPc there was a size increase to 47.03 nm.

3.2. Characterization of modified PAN fibers

The solid state UV-Vis spectra of ClInOCPc/PAN and MNP-ClInOCPc/PAN are shown in Fig. 1B. The Q band maxima for ClInOCPc/PAN and MNP-ClInOCPc/PAN were red shifted, from 689 nm in solution to ~702 nm in the solid state, Table 1. The spectra are broad due to aggregation but showed the presence of the Pc. SEM images showing fiber diameter and morphology are shown in *Supporting Information*, Fig. S3, HELION_2019-3366R3-SI.PDF). The diameter for PAN alone was 205 nm, upon embedding the Pc and conjugates, there was an increase in diameter for both ClInOCPc/PAN and MNP-ClInOCPc/PAN to 370 nm and 520 nm, respectively. We have reported such an increase in fiber diameter for Pc/MNPs electrospun fibers [22]. The SEM images also reveal that the nanofibers are cylindrical and unbranched with relatively smooth surfaces even after incorporation of the Pcs and conjugates.

The EDX spectrum of the PAN fiber alone had only the expected C and N peaks (figure not shown). Upon the introduction of the ClInOCPc there was an additional O and In, with MNP-ClInOCPc/PAN exhibiting Si and Fe confirming the presence of the MNPs, *Supporting Information*, Fig. S2B, HELION_2019-3366R3-SI.PDF).

The XRD patterns for PAN fiber show one prominent peak at approximately 17° and a weaker peak at 24°, Fig. 3B. It has been reported that the electrospun fiber produce amorphous peaks due to the rapid process of formation [23]. Following electrospinning, the sharp peaks of the ClInOCPc are lost. This was also observed for the MNP-ClInOCPc/PAN with an additional peak at 38° which is a prominent peak in magnetite.

The nitrogen adsorption-desorption isotherms for the modified PAN fiber mats are shown in Fig. 4. The surface area for PAN was 17.0 m^2/g, upon embedding the photosensitizers there was an increase to 22.6 m^2/g and 37.3 m^2/g for ClInOCPc/PAN and MNP-ClInOCPc/PAN, respectively, Table 1. There was no difference between PAN and ClInOCPc/

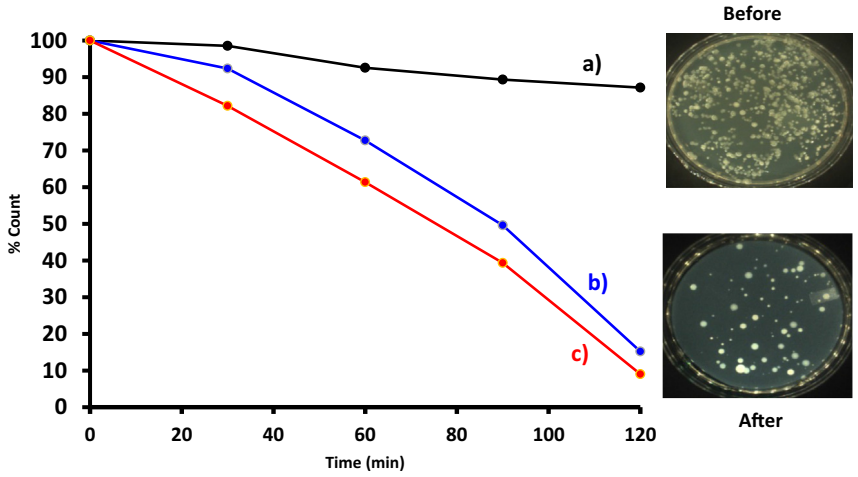

Fig. 8. Survival curves of the unknown water sample incubated with 5 μg/ml of (a) control, (b) ClInOCPc, and (c) MNP-ClInOCPc. Insert = colony forming unit photograph of the MNP-ClInOCPc sample before and after PACT.

PAN pore volume of 0.11 cm^3/g but there was an increase for MNP-ClInOCPc/PAN at 0.18 cm^3/g, Table 1. This increase of both surface area and pore volume for MNP-ClInOCPc/PAN, may be due to the presence of large magnetic nanoparticles. There was also an increase in the pore sizes from 204.6 Å for PAN to 247.5 Å and 261.9 Å for ClInOCPc/PAN and MNP-ClInOCPc/PAN, respectively.

3.3. Photochemical and photophysical parameters

3.3.1. Triplet quantum yield (Φ_T) and lifetime (τ_T)

The triplet quantum yields and lifetimes were determined for the complexes in solution. Table 1 shows that MNP-ClInOCPc has a greater Φ_T (at 0.83) compared to ClInOCPc at 0.69 in DMF, due to the presence of the heavier magnetic nanoparticle [24], which encourages intersystem crossing to the triplet state. There is an increase in the lifetime upon conjugating which can be attributed to the protection of the Pc by the MNPs.

3.3.2. Singlet oxygen quantum yield (Φ_Δ)

In this work, the Φ_Δ values were determined using 1,3-diphenylisobenzofuran (DPBF) as a singlet oxygen quencher in DMF for ClInOCPc and MNP-ClInOCPc, and anthracene-9,10-bismethylmalonate (ADMA) in water for all samples. The modified fiber was suspended (using 10 mg of ClInOCPc/PAN, MNP-ClInOCPc/PAN) in the solution containing ADMA, and irradiated using the photolysis setup described above. The decay of DPBF in DMF in the presence of ClInOCPc upon irradiation is shown in Fig. 5A. There were no changes in the intensity of the Q band of ClInOCPc in DMF, indicating stability of the Pcs and their conjugates. The photodegradation of ADMA is shown in Fig. 5B. ClInOCPc did not leach out of the fiber even though ClInOCPc is water soluble. The Φ_Δ values in DMF are 0.61 and 0.48 for ClInOCPc and MNP-ClInOCPc, respectively, Table 1. In water (containing 0.2 % DMF, since ClInOCPc and MNP-ClInOCPc are not fully soluble in water) the values are 0.41 and 0.29 for ClInOCPc and MNP-ClInOCPc, respectively, Table 1. The decrease in Φ_Δ value of MNP-ClInOCPc compared to ClInOCPc is surprising since with increase in the Φ_T, the Φ_Δ values are also expected to increase because the more populated the triplet state is, the more singlet oxygen is produced. The decrease in Φ_Δ values maybe attributed to the screening effect caused by the MNPs, which may have prevented the excited triplet state of the nanoconjugates from interacting with the ground state molecular oxygen [25]. The singlet oxygen quantum yield is lower in water compared to the studies in DMF. Oxygen has higher solubility in organic solvents compared to water [26], hence lower Φ_Δ values in the latter. For MNP-ClInOCPc/PAN and ClInOCPc/PAN suspended in water the Φ_Δ values are 0.22 and 0.36, respectively. Even though there is a decrease in Φ_Δ following conjugation of ClInOCPc to MNPs, the presence of MNPs will allow for magnetic separation following use of the conjugates for PACT or for photocatalysis, allowing for re-usability of the catalyst.

3.4. PACT studies for known bacteria (S. aureus)

The MNPs, ClInOCPc and MNP-ClInOCPc were not fully soluble in PBS (pH 7.4), to counter this they were dissolved in DMF (0.2%) to make 5 μg/ml concentration. The dark toxicity studies (Fig. 6, the error bars show the standard error where $p < 0.05$) showed that the MNPs,

Table 2
Photodynamic antimicrobial activity results of the unknown water sample.

Sample	Population inactivation (%)
Control	12.9
ClInOCPc	84.8
MNP-ClInOCPc	90.6
PAN (control)	1.8
ClInOCPc/PAN	48.0
MNP-ClInOCPc/PAN	63.7

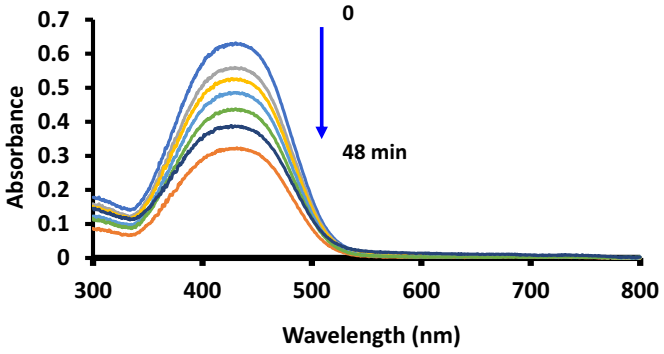

Fig. 9. Electronic absorption spectra changes 4.5 × 10^{-5} mol/L methyl red during visible light photocatalysis in the presence of ClInOCPc/PAN. pH 7.4 buffer employed.

ClInOCPc and MNP-ClInOCPc had minimal dark toxicity up until 7.5 μg/mL. The PACT (in the presence of light) activity of ClInOCPc improved in the presence of MNPs with high log values of 7.77 for MNP-ClInOCPc and 5.07 for ClInOCPc, showing that singlet oxygen quantum yields are not the only indicators for PACT activity, since it would be expected that ClInOCPc with a larger singlet oxygen quantum yield should show better PACT activity compared to MNP-ClInOCPc. The log reduction values reported here for both ClInOCPc and MNP-ClInOCPc are much larger than reported for porphyrin-Pt nanoparticle conjugates [27], where log reduction were near 3 for *S. aureus*. In addition, the use of MNPs allows for the recovery of the catalysts following use.

3.5. PACT studies for water sample with unknown bacteria

3.5.1. Optimum condition studies

The optimization of temperature and pH was adapted from previous studies [28]. The ideal temperature was determined to be 30 °C for both at 24 h and 48 h incubation, Fig. 7A, but 24 h gave larger colony forming units (CFU) hence employed for further studies. The optimum temperature was then used to optimize the pH, Fig. 7B. The pH of the water sample from the stream was found to be 6.3 and was adjusted by using acidic and basic PBS. The maximum colony count was obtained at pH 7.5 shown in Fig. 7B.

3.5.2. ClInOCPc and MNP-ClInOCPc in solution

ClInOCPc was dissolved in DMF (0.2 %) and further diluted with 7.4 PBS to make a final concentration of 5 μg/ml. The control sample (0.2% DMF in PBS) was exposed in the same irradiation conditions, but without a photosensitizer, Fig. 8 (control), and there is an insignificant change for

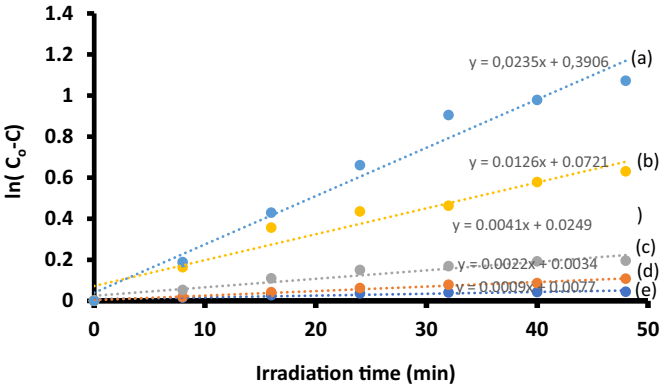

Fig. 10. First order kinetic plots for degradation methyl red: (a) 4.5 ×10^{-5}, (b) 7.9 ×10^{-5}, (c) 12.7 ×10^{-5}, (d) 15.3 ×10^{-5} and (ve) 17.2 ×10^{-5}using ClInOCPc/PAN as a catalyst. pH 7.4 buffer.

Table 3
Rates, rate constants (k_{obs}) and half-lives for methyl red degradation using ClInOCPc/PAN and MNP-ClInOCPc/PAN.

[MR] $\times 10^{-5}$ mol/L	k_{obs} (min^{-1})			Initial rate ($\times 10^{-7}$ mol L^{-1} min^{-1})			Half-life (min)		
	ClInOCPc/PAN	MNP-ClInOCPc/PAN	MNP-ClInOCPc/PAN (re-used)	ClInOCPc/PAN	MNP-ClInOCPc/PAN	MNP-ClInOCPc/PAN (re-used)	ClInOCPc/PAN	MNP-ClInOCPc/PAN	MNP-ClInOCPc/PAN (re-used)
4.5	0.0166	0.0235	0.0183	7.5	10.6	8.3	41.8	29.5	37.9
7.9	0.009	0.0126	0.0094	7.1	9.9	7.4	77.0	55.0	73.7
12.7	0.0023	0.0041	0.0032	2.9	5.2	4.1	301.4	169.1	216.6
15.3	0.002	0.0022	0.0017	3.1	3.8	2.6	346.6	315.1	407.7
17.2	0.0011	0.0009	0.0012	1.9	1.5	0.7	630.1	770.2	577.6

the control. The photodynamic antimicrobial chemotherapy studies are often reported in logarithmic reduction values to manage the high population in the stock solution and to manage the bacteria growth on the agar not to clump up. The water samples exhibited maximum CFU/ml of 1000 and therefore only 1 aliquot dilution was performed hence the results are reported in reduction percentage.

The results obtained are illustrated in Fig. 8 and summarised in Table 2. In solution the ClInOCPc was less effective with reduction percentage of 84.8 % compared to MNP-ClInOCPc at 90.6%, showing the advantage on MNPs. ClInOCPc produced a higher singlet oxygen quantum yield than the MNP-ClInOCPc, but the latter had higher PACT activity. ClInOCPc showed less stability compared with MNP-ClInOCPc, *Supporting Information*, Fig. S4, HELION_2019-3366R3-SI.PDF). This could explain the better PACT activity for the latter.

3.5.3. *ClInOCPc and MNP-ClInOCPc embedded in PAN*

The fibers were studied to observe if they could be applied in the treatment of this water sample. The embedded phthalocyanines were placed in the same agar plate as the PAN which was used as a control, the same amount of sample was inoculated and irradiated for 1 h and the reduction percentage was estimated by Eq. (1).

$$\frac{\textit{Total colony count on the embedded fibre}}{\textit{Total colony count on the control}} \times 100 \quad (1)$$

The results followed a similar trend as in solution, where the ClInOCPc/PAN is less efficient compared to MNP-ClInOCPc/PAN, Table 2.

3.6. *Photodegradation of methyl red*

The photodegradation of the methyl red was monitored by viewing the spectral changes at 8 min intervals with MNP-ClInOCPc/PAN as an example in Fig. 9.

There was a decrease in the methyl red absorption peak and the Q-band of the conjugate at the 689 nm region was not present in the spectra suggesting that the phthalocyanine did not leach out. The studies were performed at pH 7.4. Methyl red has a maximum absorbance at 425 nm, this peak has been reported as the characteristic for the dye at a pHs greater than 5.6 [29]. When the unmodified fiber were irradiated in the presence of the dye solution, there was no degradation of the methyl red (no change in absorbance), showing that the unmodified fiber does not degrade methyl red. For modified fibers, the methyl red concentration versus irradiation time plots were used to determine the kinetics, Fig. 10. The plots in Fig. 10 indicate pseudo -first order kinetics. Table 3 summarized the kinetics results. There was an increase in k_{obs} with decrease of methyl red concentration for the ClInOCPc/PAN and MNP-ClInOCPc/PAN. The MNP-ClInOCPc/PAN had a faster rate and higher k_{obs} values than ClInOCPc/PAN.

A similar trend observed for the half-lives where the values for the MNP-ClInOCPc/PAN were lower compared to the ClInOCPc/PAN, showing faster activity for the former. The MNP-ClInOCPc/PAN fiber was retrieved washed with ethyl acetate, dried and re-used for degradation of MR in solution. An increase in increase in k_{obs} with decrease of methyl red concentration was observed as was the case for the fresh MNP-ClInOCPc/PAN, however with slightly lower k_{obs} values. The SEM images showed that the fibers remained relatively unchanged following use, *Supporting Information*, Fig. S3D, HELION_2019-3366R3-SI.PDF).

4. Conclusions

ClInOCPc and MNP-ClInOCPc were successfully embedded into PAN to produce ClInOCPc/PAN and MNP-ClInOCPc/PAN, respectively. The electrospun fibers were determined to have a SEM diameter of 370 nm and 520 nm, respectively. ClInOCPc/PAN produced high singlet oxygen in water using ADMA as a quencher compared to MNP-ClInOCPc/PAN. A water sample from a local stream was tested for microbes and the fibers were applied. When in solution, MNP-ClInOCPc gave 90.6% photoinactivation of microbes in a water sample from the stream and ClInOCPc resulted in 84.8 % photoinactivation. When embedded to the polymer, there was 48.0% clearance for ClInOCPc and 63.7% clearance for MNP-ClInOCPc for the microbes in the water sample from the stream. The fibers were further used to degrade methyl red where the highest initial rates and k_{obs} were obtained by the MNP-ClInOCPc/PAN fibers with pseudo-first-order kinetics.

Declarartions

Author contribution statement

Azole Sindelo: Conceived and designed the experiments; Performed the experiments; Analyzed and interpreted the data; Wrote the paper.

Tebello Nyokong: Analyzed and interpreted the data; Contributed reagents, materials, analysis tools or data; Wrote the paper.

Funding statement

This work was supported by the Department of Science and Technology (DST) and National Research Foundation (NRF), South Africa, through DST/NRF South African Research Chairs Initiative for Professor of Medicinal Chemistry and Nanotechnology (UID 62620).

Competing interest statement

The authors declare no conflict of interest.

Additional information

Supplementary content related to this article has been published online at https://doi.org/10.1016/j.heliyon.2019.e02352.

References

[1] I. Okura, Photosensitization of Porphyrins and Phthalocyanines, Gordon and Breach Publishers, Berlin, 2001.

[2] D. Wöhrle, O. Suvorova, R. Gerdes, O. Bartels, L. Lapok, N. Baziakina, S. Makarov, A. Slodek, Efficient oxidations and photooxidations with molecular oxygen using metal phthalocyanines as catalysts and photocatalysts, J. Porphyr. Phthalocyanines 8 (2004) 1020–1041.

[3] M. Managa, M.A. Idowu, E. Antunes, T. Nyokong, Photophysicochemical behavior and antimicrobial activity of dihydroxosilicon tris(diaquaplatinum)octacarboxy phthalocyanine, Spectrochim. Acta. A. Mol. Biomol. Spectrosc. 125 (2014) 147–153.
[4] B.N. Green, C.D. Johnson, J.T. Egan, M. Rosenthal, E.A. Griffith, M.W. Evans, Methicillin-resistant Staphylococcus aureus: an overview for manual therapists, J. Chiropr. Med. 11 (2012) 64–76.
[5] M.A. Rauf, M.A. Meetani, S. Hisaindee, An overview on the photocatalytic degradation of azo dyes in the presence of TiO2 doped with selective transition metals, Desalination 276 (2011) 13–27.
[6] Ö. Çlnar, S. Yasar, M. Kertmen, K. Demiröz, N.Ö. Yigit, M. Kitis, Effect of cycle time on biodegradation of azo dye in sequencing batch reactor, Process Saf. Environ. Prot. 86 (2008) 455–460.
[7] T. Nyokong, Effects of substituents on the photochemical and photophysical properties of non-transition metal Phthalocyanines, Coord. Chem. Rev. 251 (2007) 1707–1722.
[8] C. Tshangana, T. Nyokong, Improved triplet state parameters for indium octacarboxy phthalocyanines when conjugated to quantum dots and magnetite nanoparticles, J. Mol. Struct. 1089 (2015) 161–169.
[9] E. J Viau, K.D. Goodwin, K.M. Yamahara, B.A. Layton, L.M. Sassoubre, S.L. Burns, H.-I. Tong, S.H.C. Wong, Y. Lu, A.B. Boehm, Bacterial pathogens in Hawaiian coastal streams—associations with fecal indicators, land cover, and water quality, Water Res. 45 (2011) 3279–3290.
[10] C.M. Hardina, R.S. Fujioka, Soil: the environmental source of Escherichia coli and Enterococci in Hawaii's streams, Environ. Toxicol. Water Qual. 6 (1991) 185–195.
[11] J. Ding, J. Zhang, J. Li, D. Li, C. Xiao, H. Xiao, H. Yange, X. Zhuang, X. Chen, Electrospun polymer biomaterials, Prog. Polym. Sci. 90 (2019) 1–34.
[12] J. Li, W. Xu, D. Li, T. Liu, Y.S. Zhang, J. Ding, X. Chen, Locally deployable nanofiber patch for sequential drug delivery in treatment of primary and advanced orthotopic hepatomas, ACS Nano 12 (2018) 6685–6699.
[13] M. Ambroz, A. Beeby, A.J. McRobert, M.S.C. Simpson, R.K. Svensen, D. Phillips, Preparative, analytical and fluorescence spectroscopic studies of sulphonated aluminium phthalocyanine photosensitizers, J. Photochem. Photobiol. B Biol. 9 (1991) 87–95.
[14] O.L. Osifeko, I. Uddin, P.N. Mashazi, T. Nyokong, Physicochemical and antimicrobial photodynamic chemotherapy of unsymmetrical indium phthalocyanines alone or in the presence of magnetic nanoparticles, New J. Chem. 40 (2016) 2710–2721.
[15] T. Nyokong, E. Antunes, K. Kadish, K. Smith, in: R. Guilard (Ed.), Handb. Porphyr. Sci., World Scientific Publishing Co. Pte. Ltd., Singapore, 2010, pp. 247–349.
[16] J. Kossanyi, D. Chahraoui, Electron transfer reaction and demetalation of phthalocyanines, Int. J. Photoenergy 2 (2000) 9–15.
[17] M.J. Stillman, T. Nyokong, in: A.B.C. Lever, C.C. Leznoff (Eds.), Phthalocyanines - Properties and Applications, 1, VCH, New York, 1989. Chapt. 3.
[18] C.M. Hoo, N. Starostin, P. West, M.L. Mecartney, A comparison of atomic force microscopy (AFM) and dynamic light scattering (DLS) methods to characterize nanoparticle size distributions, J. Nanoparticle Res. 10 (2008) 89–96.
[19] P. Borker, A.V. Salker, Synthesis, characterization and photocatalytic studies of some metal phthalocyanines, Indian J. Chem. Technol. 13 (2006) 341–346.
[20] A.W. Snow, J.R. Griffith, N.P. Marullo, Syntheses and characterization of heteroatom-bridged MetalFree phthalocyanine network polymers and model compounds, Macromolecules 17 (1984) 1614–1624.
[21] R. Jenkins, R.L. Synder, Introduction to X-ray Diffractometry, Wiley and Sons, New York, 1998.
[22] S. Mapukata, F. Chindeka, K.E. Sekhosana, T. Nyokong, Laser induced photodegradation of Orange G using phthalocyanine – cobalt ferrite magnetic nanoparticle conjugates electrospun in polystyrene nanofibers, Mol. Catal. 439 (2017) 211–223.
[23] H. Fong, D.H. Reneker, Elastomeric nanofibers of styrene–butadiene–styrene triblock copolymer, J. Polym. Sci. B. 37 (1999) 3488–3493.
[24] J.C. Koziar, D.O. Cowa, Photochemical heavy-atom effects, Accounts Chem. Res. 11 (1978) 334–341.
[25] E. Dube, N. Njemuwa, D.O. Oluwole, J. Mack, T. Nyokong, Investigation of photophysicochemical properties of zinc phthalocyanines conjugated to metallic nanoparticles, J. Photochem. Photobiol., A 349 (2017) 148–161.
[26] I.B. Golovanov, S.M. Zhenodarova, Quantitative structure-property relationship: XXIII. Solubility of oxygen in organic solvents, Russ. J. Gen. Chem. 75 (2005) 1795–1797.
[27] M. Managa, T. Nyokong, Photodynamic antimicrobial chemotherapy activity of gallium tetra- (4-carboxyphenyl) porphyrin when conjugated to differently shaped platinum nanoparticles, J. Mol. Struct. 1099 (2015) 432–440.
[28] L. Rosso, J.R. Lobry, S. Bajard, J.P. Flandrois, Convenient model to describe the combined effects of temperature and pH on microbial growth, Appl. Environ. Microbiol. 61 (1995) 610–616.
[29] J.-H. Zhang, Q. Liu, Y.-M. Chen, Z.-Q. Liu, C.-W. Xu, Determination of acid dissociation constant of methyl red by multi-peaks Gaussian fitting method based on UV-visible absorption spectrum, Acta Phys. - Chim. Sin. 28 (2012) 1030–1036.